INORGANIC CHEMISTRY FRONTIERS

RESEARCH ARTICLE

View Article Online
View Journal | View Issue

Cite this: *Inorg. Chem. Front.*, 2025, **12**, 7411

A new quinoline-based cobalt(II) catalyst capable of bifunctional water splitting†

Carlos A. Lucecki, ‡[a] Neha Rani,‡[a] Kenneth K. Kpogo,‡§[a] Jens Niklas, [b] Oleg G. Poluektov, [b] H. Bernhard Schlegel *[a] and Cláudio N. Verani *[a,c]

Received 23rd May 2025,
Accepted 23rd July 2025

DOI: 10.1039/d5qi01196e

rsc.li/frontiers-inorganic

We report on a new water-soluble cobalt(II) complex capable of water splitting bifunctionality, *i.e.*, water reduction and water oxidation. The species $[Co^{II}(L^{Qpy})H_2O]ClO_4$ (**1**), where L^{Qpy} is the deprotonated form of the new tripodal ligand N^1,N^1-bis(pyridin-2-ylmethyl)-N^2-(quinolin-8-yl)benzene-1,2-diamine, HL^{Qpy}, was developed aiming to replace an oxidation prone methylene group by a sturdy and redox stable quinoline. The molecular and electronic structures of **1** were evaluated by multiple spectroscopic, spectrometric, electrochemical and computational methods, and detailed pre- and post-catalytic studies were conducted to ascertain the molecular nature of the conversions. Complex **1** performs water reduction at a low onset overpotential (η) of 0.65 V at pH 7, reaching TON_{3h} 2900 (TOF 970 h^{-1}) and TON_{18h} 12 100 (TOF 672 h^{-1}) with up to 98% faradaic efficiency (FE). Species **1** also promotes water oxidation at η = 0.34 V under pH 8, achieving TON_{3h} 193 (TOF 64 h^{-1}) at 84% FE. Experimental and DFT results enabled us to propose reaction intermediates and mechanisms.

Introduction

The fundamental bottleneck of water splitting is the thermodynamic barrier of 1.23 V to convert water into dihydrogen and dioxygen.[1,2] Several species containing cobalt,[3–20] nickel,[21–25] copper,[26,27–30] and iron[31–33] have been developed aiming to seize the affordable free energies of activation (ΔG^*) displayed by 3d-based catalysts. This is related to the fact that the atomic 3d orbitals have a smaller radial extension than their 4d and 5d counterparts, yielding smaller molecular orbitals and weaker ligand fields. As a consequence, these metals foster weaker M–L bonds that yield significant challenges, which remain unsolved.[34] Because of its advantages, and in spite of its shortcomings, the ability of a single 3d-based molecular catalyst to present bifunctional activity and mediate both water reduction and oxidation is highly desirable for its potential to simplify the complexity of photoelectrochemical cell processes. To the best of our knowledge, only a few bifunctional water splitting molecular complexes are known,[35–38] as most advances in this field have been achieved using heterogeneous systems.[39,40] This likely stems from the fact that water oxidation and water reduction catalysts typically require distinct ligand environments: highly active oxidation catalysts are often based on resistant, non-innocent ligands that withstand harsh oxidative conditions.[15,16,30] In contrast, effective reduction catalysts rely on flexible ligands that facilitate the formation of low-valent metal species capable of proton reduction.[41–43] Considering the relevance of $Co[N_5]$ platforms, our groups have discussed how ligand architecture influences the activity of tripodal methyl-pyridine-based cobalt catalysts in proton and water reduction[12] for the species $[Co^{II}(L^{Py})]^{2+}$ (Scheme 1a). The ligand framework was prone to oxygen insertion to the singly substituted Ph–NH–CH_2Py leading to eventual

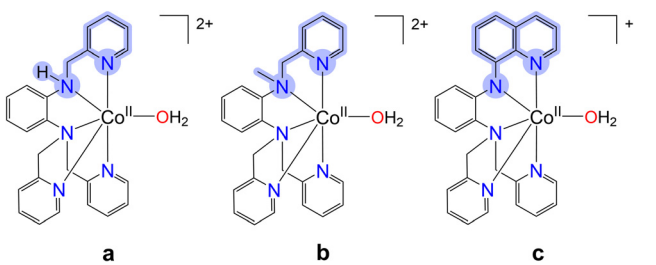

Scheme 1 Co-based catalysts with tripodal $[N_5]$ platforms. (a) $Co[N_5]$ with exposed oxidation-prone methylene. (b) Protected methylated amine. (c) New quinoline-based $Co[N_5]$.

[a]*Department of Chemistry, Wayne State University, 5101 Cass Avenue, Detroit, Michigan 48202, USA. E-mail: claudio.verani@wayne.edu*
[b]*Argonne National Laboratory, 9700 South Cass Ave, Lemont, Illinois 60439, USA*
[c]*Department of Chemistry and Biochemistry, University of Windsor, 401 Sunset Avenue, Windsor, Ontario N9B 3P4, Canada*

†Electronic supplementary information (ESI) available. CCDC 2401035. For ESI and crystallographic data in CIF or other electronic format see DOI: https://doi.org/10.1039/d5qi01196e

‡These authors contributed equally to the development of this work.

§Current address: Moses Lake Industries, Moses Lake, Washington 98837, United States.

decomposition. This methylene oxidation is a common limitation for molecular catalysts,[33,44–46] and leads to CoOx nanoparticulates that are less tuneable or selective. The doubly substituted Ph–N(–$CH_2Py)_2$ moiety was more resilient to oxidation and led us to incorporate a methyl protecting group to the singly substituted amine with good results ($[Co^{II}(L^{MePy})]^{2+}$, Scheme 1b). The latter displayed significant catalytic efficiency towards water reduction with TON_{18h} of 6000 (TOF 333 h^{-1}).

Here, we hypothesize that the incorporation of a more robust singly substituted framework, such as a quinoline, will prevent oxygen insertion while enhancing catalytic activity by enabling electron shuffling within the framework (Scheme 1c). Replacing the susceptible methylene group with a non-innocent ligand moiety may not only prevent ligand oxidation,[47] but also stabilize low- and high-valent states relevant for water reduction and oxidation, thus yielding a truly bifunctional water splitting catalyst.

Results and discussion

Syntheses and characterizations

The new HL^{Qpy} ligand was obtained by reacting N^1-(quinolin-8-yl)benzene-1,2-diamine[48,49] (Fig. S1†) with picolyl chloride in water containing sodium hydroxide and catalytic amounts of hexadecyl-trimethyl-ammonium chloride. The complex $[Co^{II}(L^{Qpy})H_2O]ClO_4$ (**1**) (Scheme 1c) was then synthesized by treating one equivalent of HL^{Qpy} with one equivalent of Co $(ClO_4)_2{\cdot}6H_2O$ in the presence of triethylamine in methanol. The complex and the ligand HL^{Qpy} were characterized by ^1H NMR (Fig. S2†), ESI-MS (Fig. S3 and S4†), FTIR and elemental analysis (see Experimental section for details), as well as X-ray crystallography. Species **1** yielded high-quality crystals and its structure is in agreement with other techniques. ESI-MS results show a characteristic peak at m/z = 476.0 for **1**. FTIR displays a series of bands related to the pyridyl groups between 1340–1610 cm^{-1}. Complex **1** also exhibited a sharp peak at 1090 cm^{-1} attributed to the perchlorate counterion.

Molecular structure

The identity of the new ligand and complex are shown in Fig. 1 and reveal that **1** crystallizes as a dimer with a *trans-μ*-peroxo bridge between the two Co centres, where each Co site displays a pseudo-octahedral environment. The Co–N bond lengths span 1.88–2.00 Å, whereas the Co–O bonds are ~1.87 Å in length. The unit cell contains two uncoordinated ClO_4^- counterions suggesting a Co^{III} oxidation state for the metal centres. It is important to mention that the dimer results from adventitious oxidation of the complex during crystallization under ambient conditions and *does not* represent an intermediate in the mechanism by which dioxygen is generated. Selected crystallographic bond lengths are provided in Table T5.†

Electronic structure

The electronic behaviour of the ligand HL^{Qpy} and of species **1** was investigated by UV–visible spectroscopy and further supported by time-dependent DFT (TD-DFT) calculations along with the natural transition orbital (NTO) analysis.[50–53] The ligand displays two bands at 260 nm (ε = 38 600 L mol^{-1} cm^{-1}) and 380 nm (9800 L mol^{-1} cm^{-1}) that are characterized as intraligand charge transfer (ILCT) processes by TD-DFT (Fig. S5–S7†). Complex **1** shows a decreased ILCT band at 260 nm (24 300 L mol^{-1} cm^{-1}) upon metal coordination (Fig. 2a and Fig. S8†). New bands appear at 308 nm (24 100 L mol^{-1} cm^{-1}) and 500 nm (6000 L mol^{-1} cm^{-1}). The TD-DFT calculations identify these as ILCT processes (Fig. 2a and Fig. S8, S9†).[54] The calculations also find MLCT and LMCT bands but the oscillator strengths for these transitions are too low to be visible in the spectrum.

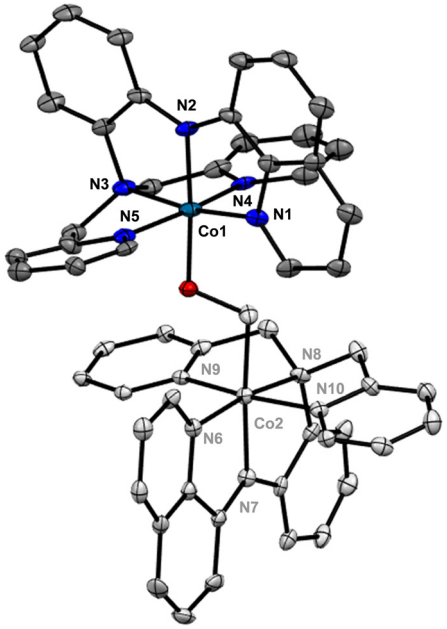

Fig. 1 ORTEP representation of the dimeric oxidized form of **1** (CCDC 2401035†) at 20% probability. H atoms are omitted and only one unit is highlighted for clarity.

Four independent redox events were observed by cyclic voltammetry (CV), consisting of two reductive and two oxidative processes (Fig. 2b and S10†). All the potentials are reported *versus* Ag/AgCl and summarized in Table T1.† A metal-based process associated with the Co^{II}/Co^{I} couple is seen around E_{pc} = −0.30 V. It is possible to observe two quasi-reversible processes at $E_{1/2}$ = −1.55 V (ΔE_p = 100 mV) and at $E_{1/2}$ = 0.94 V (ΔE_p = 100 mV), tentatively assigned to ligand reduction and to the Co^{III}/Co^{II}, respectively.[55,56] The anodic reversible process at $E_{1/2}$ = 1.34 V (ΔE_p = 60 mV) has been characterized as ligand oxidation (*vide infra*).

To further characterize the electronic structure of **1**, we performed a series of one- and two-electron oxidation experiments *via* bulk electrolysis (BE). The oxidized products were then analysed by electron paramagnetic resonance (EPR) as shown in Fig. 2c (see the Experimental section for more details). The EPR spectrum of the parent complex **1** is typical for a high-spin $3d^7$ $^{HS}Co^{II}$ species (S = 3/2), with no indication of a low-

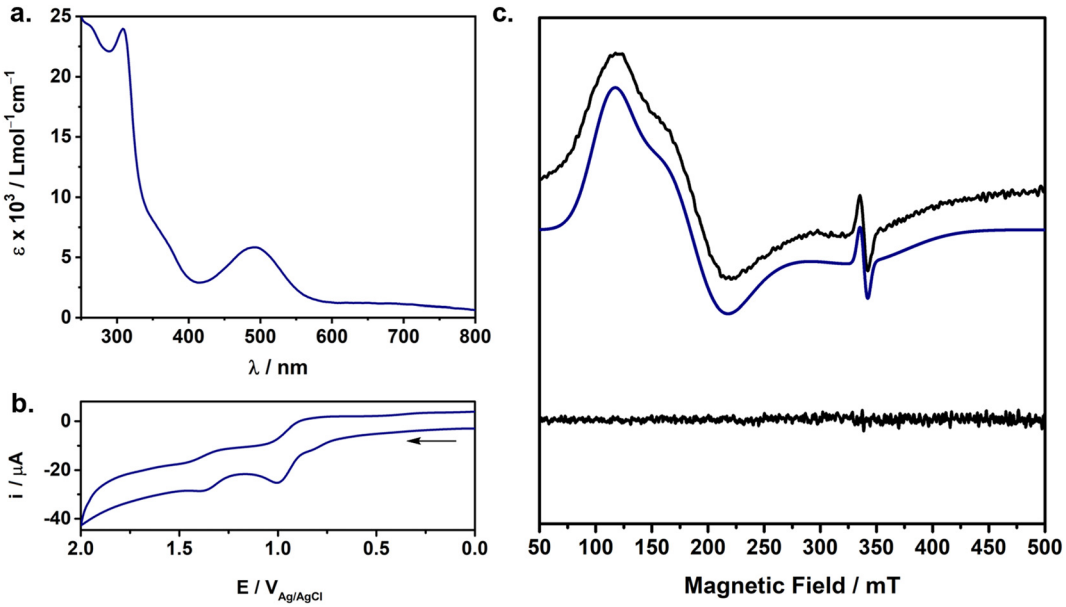

Fig. 2 (a) UV–visible spectrum of **1** in acetonitrile. (b) CV of **1** in acetonitrile (1.0×10^{-3} mol L^{-1}). $TBAPF_6$ as supporting electrolyte (0.1 mol L^{-1}), glassy carbon (WE), Pt wire (CE) and Ag/AgCl (RE). Scan rate: 100 mV s^{-1}. (c) Continuous wave (cw) X-band (9.48 GHz) EPR spectra of **1** at T = 30 K. Parent species (top), and one-electron oxidized species (bottom). The experimental and simulated data are presented as black and blue traces, respectively.

spin configuration.[12,57] The peaks are interpreted as transitions between the $m_s = \pm 1/2$ sublevels and can be simulated (blue trace) as an effective $S = 1/2$ system with $g_1 = 5.85$, $g_2 = 3.57$, and $g_3 = 1.96$. These values align with those reported for analogous $^{HS}Co^{II}$ platforms.[12] The small signal observed at 340 mT ($g \approx 2$, <0.1%) is attributed to a minor amount of an organic radical. Therefore, the simulated spectrum of the parent species represents a sum of contributions from a $^{HS}Co^{II}$ species and a $g = 2.00$ species (Fig. S11†). The $1e^-$ oxidized sample lacks an EPR signal and confirms the presence of a closed-shell low-spin $3d^6$ $^{LS}Co^{III}$ ($S = 0$) diamagnetic species. An attempt to isolate the $2e^-$ oxidized species yielded a weak and noisy spectrum of difficult interpretation, possibly associated with the short-lived nature of the product.

Bifunctional electrocatalytic activity

Water reduction. $[Co^{II}(L^{Qpy})H_2O]ClO_4$ (**1**) was evaluated towards dihydrogen production in aqueous phosphate buffer (0.1 mol L^{-1}) at pH 7 using a Hg-pool working electrode (Fig. 3). Remarkably, a strong catalytic current starting at −1.20 V (η = 0.65 V) followed by the evolution of bubbles was observed upon addition of **1**. Bulk electrolysis was performed to evaluate the catalytic performance of **1** on water reduction (inset in Fig. 3). Following 3 h of electrolysis at an applied potential of −1.70 V, species **1** yielded a turnover number TON_{3h} = 2900, turnover frequency TOF = 970 h^{-1} with no apparent loss in activity at faradaic efficiency, %FE = 98%. The high %FE indicates that nearly every electron transferred is utilized in the production of H_2. Bulk electrolysis was also monitored for 18 h to probe catalyst robustness (Fig. S12†), thus

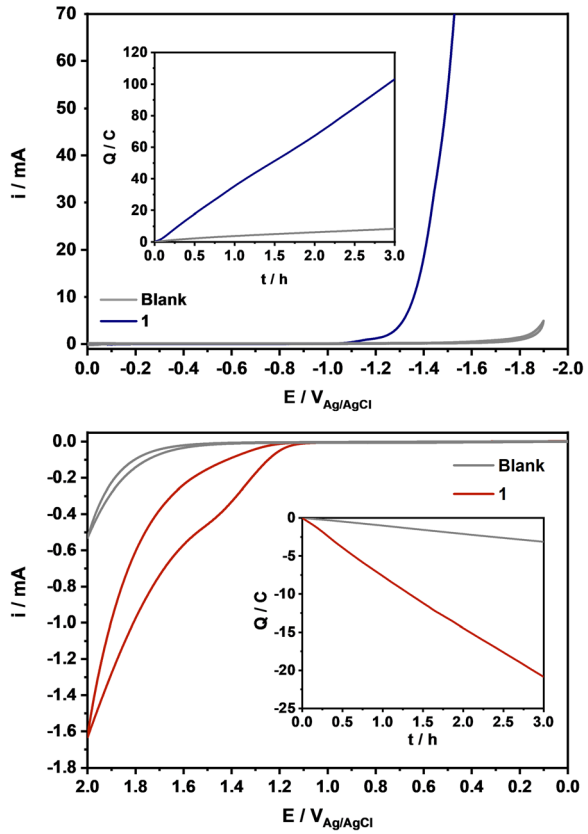

Fig. 3 Top: polarization curve of **1** in 0.1 mol L^{-1} phosphate buffer at pH 7. Inset displays a charge *vs.* time plot of **1** during bulk electrolysis at −1.70 V. Bottom: polarization curve of **1** in 0.1 mol L^{-1} borate buffer at pH 8. Inset displays a charge *vs.* time plot of **1** during bulk electrolysis at 1.50 V.

resulting in an impressive TON of 12 100, TOF of 672 h^{-1} and %FE of 97%. Control experiments conducted without the catalyst produced negligible amounts of H_2. These results validate the viability of **1** as a stable and effective catalyst for water reduction. In addition, TON and TOF values imply that **1** yields better results than those reported for analogous cobalt catalysts under similar experimental conditions.[12,36,58,59] As shown in Table T8 of the ESI,† replacing the methylene group in $[Co^{II}(L^{MePy})]^{2+}$ with a quinoline results in a 50 mV decrease in overpotential for complex **1**. This modification not only enhances catalytic efficiency (with a twofold increase in TON) but also improves catalyst robustness, reflected by a 2.1% relative increase in %FE. This supports our central hypothesis that a non-innocent ligand contributes to stabilizing key reaction intermediates.

In order to ascertain the molecular identity of **1** as the *de facto* catalyst, post-catalytic UV–visible spectroscopy, scanning electron microscopy (SEM), and energy dispersive X-ray spectroscopy (EDS) were performed and compared to pre-catalytic data. Excellent agreement was observed between pre-catalytic (1.0 mol L^{-1}, pH 7) and post-catalytic UV–visible spectra in phosphate buffer, with only a slight increase of <4% in the 300 nm and <2% increase in the 450 nm bands (Fig. 4a). Distortion of the framework of **1** should suffice to account for this difference. To further confirm the homogeneity of the reaction, bulk electrolysis was performed using a conductive grafoil sheet as the working electrode. By replacing the Hg-pool electrode with a solid state one, we can trap adventitious nanoparticulates resulting from catalyst decomposition.[60] Although SEM images (Fig. 4b) have shown the formation of some particulate, EDS analyses used to determine its elemental composition indicated the presence of carbon, sodium, and phosphorus, (Fig. S13†), likely associated with the grafoil electrode and the phosphate buffer. No cobalt was found. Hence, the absence of cobalt or cobalt oxides on the electrode suggests that water reduction was, indeed, promoted by the molecular complex **1**.

Water oxidation. To assess the capability of **1** to perform water oxidation, and therefore act as a truly bifunctional catalyst, a polarization curve was obtained in borate buffer (0.1 mol L^{-1}, pH 8) using a fluorine-doped tin oxide (FTO, $A \approx 1.3$ cm^2) substrate as the working electrode (Fig. 3). After scanning the borate buffer in the absence of the catalyst, a minor catalytic wave (j_{cat} = −0.41 mA cm^{-2}) was observed rising from 1.50 to 2.00 V. Upon addition of **1**, an oxidation peak was observed, followed by a robust catalytic wave (j_{cat} = −1.26 mA cm^{-2}), which resulted in an onset overpotential of η = 0.34 V. We tentatively assign the increase in current at *ca.* 1.58 V to the formation of a putative "Co^{IV} state", which could entail a high-oxidation metal ion in $[Co^{IV}(L^{Qpy})]$, or its equivalent

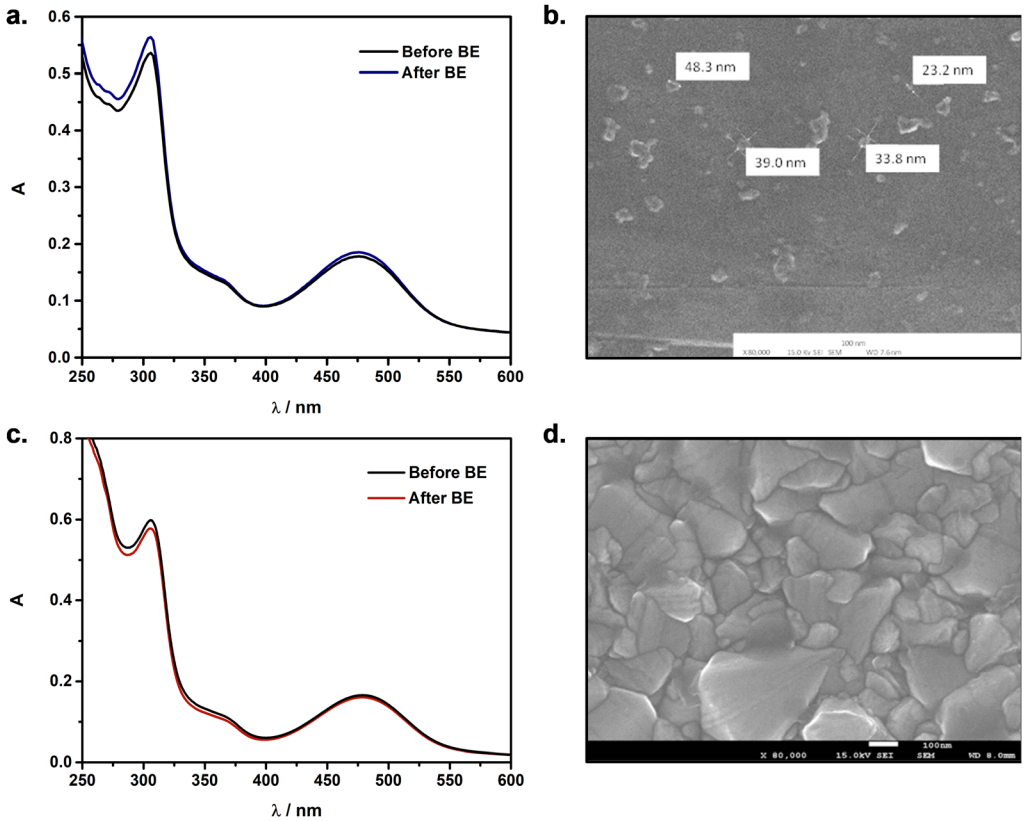

Fig. 4 (a) UV–visible spectra of **1** before and after 18 h of bulk electrolysis at −1.70 V. (b) SEM of the grafoil electrode surface after electrolysis. (c) UV–visible spectra of **1** before and after 3 h of bulk electrolysis at 1.50 V. (d) SEM of the FTO electrode surface after electrolysis.

ligand-based valence tautomer $[Co^{III}(L^{Qpy\bullet+})]$.[13] Bulk electrolysis was performed under the same conditions, using a constant potential of 1.50 V for 3 and 18 h. Complex **1** displays a linear charge *vs.* time plot with no substantial loss in activity in the first 3 h (inset in Fig. 3), revealing a TON_{3h} of 193, and TOF of 64 h^{-1} at %FE 84. The prolonged 18 h electrolysis seems to lead to catalyst decomposition, as detailed later. A comparison of the efficiency of **1** with other Co-based platforms for water oxidation is also provided in Table 8 of the ESI.†

In a similar way as for water reduction, comprehensive post-catalytic analyses were performed after water oxidation to ascertain the identity of the active catalyst. SEM, EDS and X-ray photoelectron spectroscopy (XPS) analyses were used to characterize the morphology and composition of the surface of FTO glass. The SEM images collected before and after bulk electrolysis show no changes in the morphology of the electrode (Fig. 4d). The absence of electrodeposition onto the FTO glass suggests that **1** remains a stable molecular entity in solution. More evidence for the homogeneity of the reaction comes from EDS and XPS analyses, where no traces of cobalt were found onto the electrode (Fig. S14 and S15†). The nature of **1** was also probed by comparing the electronic spectra before and after electrocatalysis. As shown in Fig. 4c, the catalyst keeps its original features after being exposed to an oxidative potential for 3 h. We conclude that while the data support a molecular mechanism for water oxidation within the first 3 h, the molecular catalyst undergoes decomposition following 18 h of bulk electrolysis. Subsequent analyses using XPS (Fig. S15 and S16†), SEM, and EDS (Fig. S17 and S18†) indicate electrodeposition of mixed cobalt oxides onto the FTO glass. This deactivation pathway typically involves a combination of ligand degradation and demetallation, ultimately leading to the formation of metal oxides.[44,47] UV–visible spectroscopy further confirms the disappearance of characteristic molecular charge-transfer bands in the post electrolysis (Fig. S19†). Consequently, this deactivating mechanism hinders the calculation of catalytic parameters.

Mechanistic insights. With these experimental results at hand, we proceeded to evaluate possible mechanisms for both water reduction and water oxidation. Fig. 5 presents these schematic pathways, which are marked by excellent agreement between experimental and DFT calculated findings. The catalytic cycles for the generation of both H_2 and O_2 are initiated with species $[Co^{II}(L^{Qpy})H_2O]^+$ (**1**). The generation of H_2 requires the loss of water and formation of $[Co^{II}(L^{Qpy})]^+$ (**2**). Species **1** and **2** readily interconvert in the presence of an aqueous solvent, where the energy change (ΔE) is affordable at 7.2 kcal mol^{-1}. The water reduction cycle begins with the reduction of the $3d^7$ metal to a low-valent state. As shown on the left side of Fig. 5 the water reduction catalytic cycle starts with a penta-

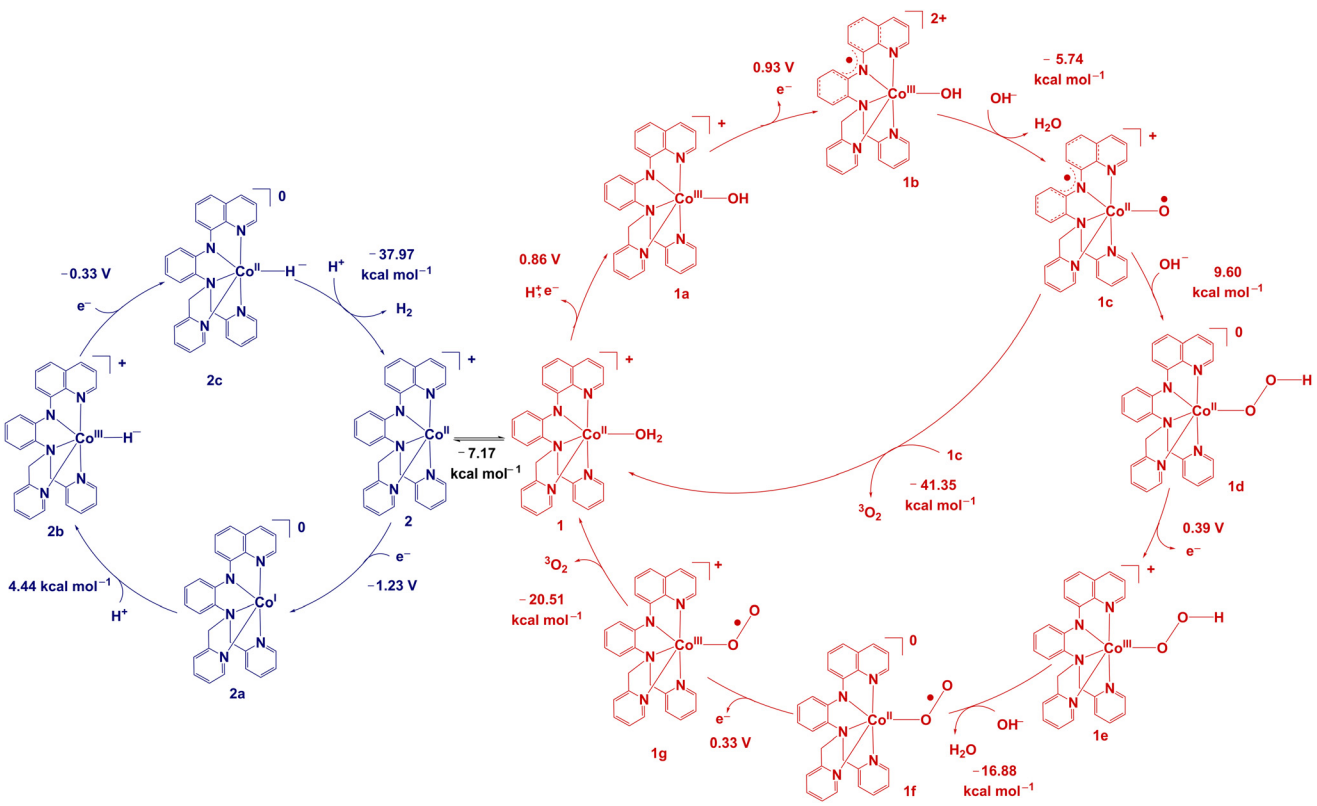

Fig. 5 Water-reduction and water-oxidation mechanisms proposed for catalyst $[Co^{II}(L^{Qpy})H_2O]ClO_4$ (**1**). Results based on comparative experimental and DFT-calculated (B3PW91/SDD/6-31G**) data. The energies (ΔG) are reported in kcal mol^{-1} and the potentials *versus* Ag/AgCl. Calculated potentials with respect to the Fc^+/Fc couple can be found in Table T2 of the ESI.†

coordinate **2**, where amine, polypyridine and quinoline donors are bound to the Co^{II} ion *via* nitrogen atoms. The high-spin $3d^7$ configuration of **2**, calculated as a quartet (S = 3/2), was 13.9 kcal mol^{-1} more stable than the low-spin doublet state with an S = 1/2. The Mulliken Spin Density (MSD) value of 2.62 on the metal centre supports the presence of an authentic $^{HS}3d^7$ Co^{II} ion (Fig. 6), in excellent agreement with the EPR data shown in Fig. 2c. Reduction of **2** yields a $3d^8$ Co^{I} intermediate, **2a**, at a potential of −1.23 V. Subsequent binding of a proton to the Co^{I} complex gives rise to the Co^{III}–H^- hydride **2b** species. This step requires an energy input of 4.4 kcal mol^{-1}. A second electron reduction, from Co^{III}–H^- to Co^{II}–H^- (**2b** to **2c**), occurs at −0.33 V. The Co^{II}–H^- intermediate **2c** can then further combine with another proton to yield dihydrogen gas. The release of H_2 and the regeneration of the initial catalyst **2** are significantly favoured by −37.9 kcal mol^{-1}. These results are in good agreement with our previous work, in which metal-based hydride formation is favoured by such cobalt complexes,[12,14,61,62] with no evidence of relay mechanisms observed in analogous nickel and copper catalysts.[63,64]

We propose that the water oxidation cycle (right side of Fig. 5) starts with the $^{HS}3d^7$ $[Co^{II}–OH_2]^+$ species **1**. As shown in Fig. 6, the Co^{II} centre in **1** has an MSD value of 2.62, confirming the presence of an authentic high-spin $3d^7$ $^{HS}Co^{II}$. Complex **1** undergoes a proton-coupled electron transfer (PCET) step to yield the closed-shell $3d^6$ $[Co^{III}–OH]^+$ diamagnetic intermediate **1a**. The oxidation event is localized almost exclusively on the metal centre with little involvement of the ligand at a calculated potential of 0.86 V. This is further supported by EPR (Fig. 2c), in which the one-electron oxidized sample is EPR–silent, consistent with a low-spin $3d^6$ Co^{III} (S = 0) species. The deprotonation of the singlet **1a** to yield the singlet $[Co^{III}–O]^0$ intermediate is uphill by 19.20 kcal mol^{-1}, making it a highly unfavourable step (Fig. S21†). A second oxidation at 0.93 V generates the $[L^{\bullet}–Co^{III}–OH]^{2+}$ species (**1b**), indicating that this redox event is centred on the ligand backbone. The computed MSD of 1.01 on the ligand in **1b** (Fig. 6) confirms the generation of a ligand-centred radical, consistent with the second oxidative wave observed in the CV (Fig. 2b). The high-spin (S = 5/2) state of **1b** is 15.28 kcal mol^{-1} higher in energy (ΔG) than the low-spin doublet (S = 1/2) configuration (Table T6†). The doublet complex **1b** can undergo deprotonation at an energy of −5.74 kcal mol^{-1}, leading to the formation of species **1c**, $[L^{\bullet}–Co^{II}–O^{\bullet}]^+$. An alternative pathway to form **1c** involves an initial spin-conserved (S = 1/2) deprotonation from **1b**, followed by a transition from the doublet to the quintet state **1c**, both steps being energetically favourable (Fig. S21†). The high-spin (S = 5/2) state of **1c** is more stable by 7.10 kcal mol^{-1} compared to the low-spin (S = 1/2) state (Table T6†). Notably, the spin-conserved deprotonation step is far more accessible from the doubly charged $[L^{\bullet}–Co^{III}–OH]^{2+}$ intermediate (**1b**) than from the mono-cationic $[Co^{III}–OH]^+$ **1a**. These steps, while described individually, may in fact occur concertedly or in a partially concerted manner under catalytic conditions. The intermediate **1c** can potentially combine with another $[L^{\bullet}–Co^{II}–O^{\bullet}]^+$ species in solution, yielding a dioxygen molecule and regenerating the $^{HS}3d^7$ Co^{II} species **1**. This step is energetically favourable by 41.3 kcal mol^{-1}. Alternatively, the species **1c** is susceptible to an OH^- attack in basic medium, leading to formation of the hydroperoxo $[Co^{II}–O–O–H]^0$ intermediate **1d**. This process is slightly uphill, requiring 9.60 kcal mol^{-1}. Species **1d** can undergo a one-electron oxidation at 0.39 V to yield $[Co^{III}–O–O–H]^+$ (**1e**). Complex **1e** is then deprotonated at an energy of −16.9 kcal mol^{-1}, leading to the formation of the superoxide $[Co^{II}–O–O^{\bullet}]^0$ species (**1f**). This species can be alternatively, obtained through direct PCET from **1d** at a potential of −0.34 V. Another one-electron oxidation event available to species **1f** leads to the formation of a superoxide $[Co^{III}–O–O^{\bullet}]^+$ intermediate (**1g**) at 0.33 V. Release of $^3O_2$ then occurs, regenerating the starting complex **1** and is highly favourable with a calculated energy of −20.5 kcal mol^{-1}. These pathways align with accepted mechanisms for water oxidation[11,65–68] and with a recent study from our groups on a tripodal imidazole/pyridine catalyst.[36] In that case, most of the activity was attributed to the ligand, with the metal center remaining in the Co(II) or Co(III) oxidation states throughout the catalytic cycle.

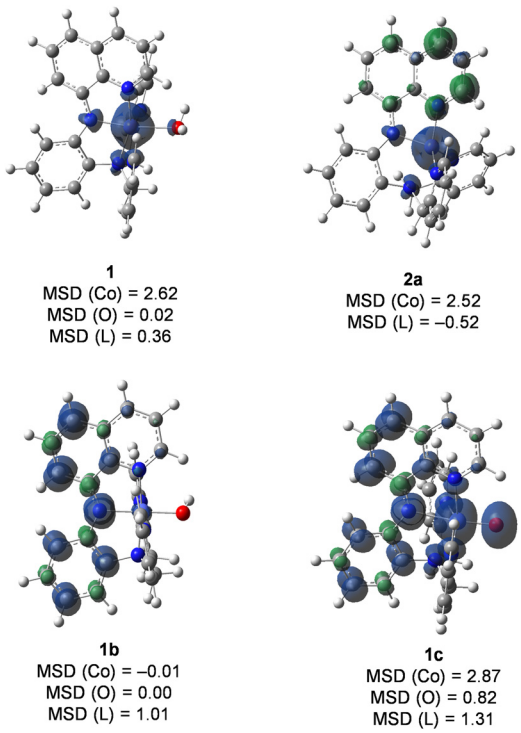

Fig. 6 Spin density plots with Mulliken Spin Density (MSD) (isovalue = 0.004 a.u.) values of the calculated structures **1**, **2a**, **1b** and **1c**. The corresponding structures are shown in Fig. 5.

Conclusions

In conclusion, we synthesized and characterized the asymmetric pentadentate complex $[Co^{II}(L^{Qpy})H_2O]ClO_4$ (**1**) based on

the new ligand platform HL^{Qpy} containing quinolyl-bispyridine moieties. This new complex behaves as a bifunctional catalyst for both water reduction and water oxidation. In both cases, a multitude of experimental methods support the molecular form of **1** as the catalytically active species without loss in activity, ligand degradation or demetallation. This was observed for water reduction at 3 and 18 h and for water oxidation at 3 h, while longer water oxidation periods of 18 h led to decomposition. While the mechanistic pathways for water reduction seem in good agreement with other cobalt catalysts from our labs, determination of the pathways for water oxidation required more effort. Current research in our group aim to extend the use of this quinoline-based HL^{Qpy} platform to other abundant 3d metal ions, and to expand the design of new doubly and triply substituted quinoline ligands for photocatalytic studies. Results will follow.

Conflicts of interest

There are no conflicts to declare.

Data availability

The data that support the findings of this study are available in the ESI† of this article, such as experimental details, syntheses and characterizations, post-catalysis studies and DFT calculations. Crystallographic data for the oxidized dimeric form of complex **1** have been deposited at the Cambridge Crystallographic Data Centre (CCDC) under accession number 2401035.† This data is available without specific restrictions, in accordance with the journal's standard access policies.

Acknowledgements

C. N. V. thankfully acknowledges support from the U.S. Department of Energy (DOE-BES) through the grant DEFOA0002414, and from the Natural Sciences and Engineering Research Council of Canada (NSERC) through the Discovery Grant RGPIN-2025-06312. H. B. S. acknowledges support from the National Science Foundation (NSF) through grant CHE1856437. C. N. V. and H. B. S. also acknowledge funding from a previous collaborative grant (DOE-BES DE-SC0001907 and DE-FG02-09ER16120). J. N. and O. G. P. acknowledge support from the U.S. Department of Energy, Office of Science, Office of Basic Energy Sciences, Division of Chemical Sciences, Geosciences, and Biosciences, under contract number DE-AC02-06CH11357 at Argonne National Laboratory. The authors acknowledge the WSU-Computing Grid for access to their facilities and Dr Sameera Perera for assistance with XPS data fitting and interpretation. This work made use of the UPS/XPS that is partially funded by the National Science Foundation #1849578.

References

1 L.-H. Zhang, S. Mathew, J. Hessels, J. N. H. Reek and F. Yu, Homogeneous Catalysts Based on First-Row Transition-Metals for Electrochemical Water Oxidation, *ChemSusChem*, 2021, **14**, 234–250.
2 S. Karim, N. Tanwar, S. Das, R. Ranjit, A. Banerjee, Gulafshan, A. Gupta, A. Kumar and A. Dutta, Shaping the Future of Green Hydrogen Production: Overcoming Conventional Challenges with Molecular Catalysts, Immobilization, and Scalable Electrolyzers, *ACS Catal.*, 2025, **15**, 1073–1096.
3 P. Wang, N. Le, J. D. McCool, B. Donnadieu, A. N. Erickson, C. E. Webster and X. Zhao, Photocatalytic Hydrogen Production with A Molecular Cobalt Complex in Alkaline Aqueous Solutions, *J. Am. Chem. Soc.*, 2024, **146**, 9493–9498.
4 K. Yamauchi, K. Kawano, K. Yatsuzuka, K. Kawamura, M. Kan and K. Sakai, Viologen-Radical-Driven Hydrogen Evolution from Water Catalyzed by Co-NHC Catalysts: Radical Scavenging by Nitrate and Volmer-Heyrovsky-like CPET Pathway, *J. Am. Chem. Soc.*, 2025, **147**, 5602–5614.
5 Q. Huang, J. Chen, P. Luan, C. Ding and C. Li, Understanding the factors governing the water oxidation reaction pathway of mononuclear and binuclear cobalt phthalocyanine catalysts, *Chem. Sci.*, 2022, **13**, 8797–8803.
6 S. Nestke, J. Stubbe, R. Koehler, E. Ronge, U. Albold, W. Vioel, C. Jooss, B. Sarkar and I. Siewert, A Binuclear Cobalt Complex in the Electrochemical Water Oxidation Reaction, *Z. Anorg. Allg. Chem.*, 2022, **648**, e202200119.
7 X. Hu, B. S. Brunschwig and J. C. Peters, Electrocatalytic Hydrogen Evolution at Low Overpotentials by Cobalt Macrocyclic Glyoxime and Tetraimine Complexes, *J. Am. Chem. Soc.*, 2007, **129**, 8988–8998.
8 P.-A. Jacques, V. Artero, J. Pécaut and M. Fontecave, Cobalt and nickel diimine-dioxime complexes as molecular electrocatalysts for hydrogen evolution with low overvoltages, *Proc. Natl. Acad. Sci. U. S. A.*, 2009, **106**, 20627–20632.
9 J. P. Bigi, T. E. Hanna, W. H. Harman, A. Chang and C. J. Chang, Electrocatalytic reduction of protons to hydrogen by a water-compatible cobalt polypyridyl platform, *Chem. Commun.*, 2010, **46**, 958–960.
10 S. Losse, J. G. Vos and S. Rau, Catalytic hydrogen production at cobalt centres, *Coord. Chem. Rev.*, 2010, **254**, 2492–2504.
11 D. J. Wasylenko, C. Ganesamoorthy, J. Borau-Garcia and C. P. Berlinguette, Electrochemical evidence for catalytic water oxidation mediated by a high-valent cobalt complex, *Chem. Commun.*, 2011, **47**, 4249.
12 D. Basu, S. Mazumder, X. Shi, H. Baydoun, J. Niklas, O. Poluektov, H. B. Schlegel and C. N. Verani, Ligand Transformations and Efficient Proton/Water Reduction with Cobalt Catalysts Based on Pentadentate Pyridine-Rich Environments, *Angew. Chem., Int. Ed.*, 2015, **54**, 2105–2110.
13 H. Baydoun, S. Mazumder, H. B. Schlegel and C. N. Verani, Deactivation of a Cobalt Catalyst for Water Reduction

through Valence Tautomerism, *Chem. – Eur. J.*, 2017, **23**, 9266–9271.
14 F. Morgan, R. Schaugaard, D. Anderson, H. B. Schlegel and C. N. Verani, Distinct Bimetallic Cooperativity Among Water Reduction Catalysts Containing [CoIIICoIII], [NiIINiII], and [ZnIIZnII] Cores, *Chem. – Eur. J.*, 2022, **28**, e202104426.
15 A. Ali, A. Das, A. Santra, R. Kumar Verma and S. Paria, Redox Non-Innocent Ligand Assisted Electrocatalytic Water Oxidation Catalyzed by a Molecular Cobalt Complex, *ChemCatChem*, 2025, **17**, e202500652.
16 M. Bera, S. Kaur, K. Keshari, D. Moonshiram and S. Paria, Characterization of Reaction Intermediates Involved in the Water Oxidation Reaction of a Molecular Cobalt Complex, *Inorg. Chem.*, 2022, **61**, 21035–21046.
17 Y. Chen, X. Meng, X. Chen, X. Li, H. Ye, S. Liu, Z. Ruan, X. Liang and J. Lin, Homogeneous electrochemical water oxidation catalyzed by cobalt complexes with an amine–pyridine ligand, *Sustainable Energy Fuels*, 2023, **7**, 242–247.
18 Y.-H. Wang, Y.-J. Tseng, S. V. Kumbhar, H.-T. Chang, T. Yang, I.-C. Lu and Y.-H. Wang, Overcoming the Tradeoff Between Reaction Rate and Overpotential in Dinuclear Cobalt Complex Catalyzed Electrochemical Water Oxidation, *Chem. – Eur. J.*, 2025, **31**, e202403583.
19 H.-Y. Du, S.-C. Chen, X.-J. Su, L. Jiao and M.-T. Zhang, Redox-Active Ligand Assisted Multielectron Catalysis: A Case of CoIII Complex as Water Oxidation Catalyst, *J. Am. Chem. Soc.*, 2018, **140**, 1557–1565.
20 S. Biswas, S. Bose, J. Debgupta, P. Das and A. N. Biswas, Redox-active ligand assisted electrocatalytic water oxidation by a mononuclear cobalt complex, *Dalton Trans.*, 2020, **49**, 7155–7165.
21 N. El Harakeh, A. C. P. de Morais, N. Rani, J. A. G. Gomez, A. Cousino, M. Lanznaster, S. Mazumder and C. N. Verani, Reactivity and Mechanisms of Photoactivated Heterometallic [RuIINiII] and [RuIINiIIRuII] Catalysts for Dihydrogen Generation from Water, *Angew. Chem., Int. Ed.*, 2021, **60**, 5723–5728.
22 J. Shen, M. Wang, T. He, J. Jiang and M. Hu, Influence of the backbone of N_5-pentadentate ligands on the catalytic performance of Ni(ii) complexes for electrochemical water oxidation in neutral aqueous solutions, *Chem. Commun.*, 2018, **54**, 9019–9022.
23 J. Lin, P. Kang, X. Liang, B. Ma and Y. Ding, Homogeneous electrocatalytic water oxidation catalyzed by a mononuclear nickel complex, *Electrochim. Acta*, 2017, **258**, 353–359.
24 D. J. Martin, B. D. McCarthy, C. L. Donley and J. L. Dempsey, Electrochemical hydrogenation of a homogeneous nickel complex to form a surface adsorbed hydrogen-evolving species, *Chem. Commun.*, 2015, **51**, 5290–5293.
25 R. Tatematsu, T. Inomata, T. Ozawa and H. Masuda, Electrocatalytic Hydrogen Production by a Nickel(II) Complex with a Phosphinopyridyl Ligand, *Angew. Chem., Int. Ed.*, 2016, **55**, 5247–5250.
26 S. Chattopadhyay, A. Ghatak, Y. Ro, R. Guillot, Z. Halime, A. Aukauloo and A. Dey, Ligand Radical Mediated Water Oxidation by a Family of Copper o-Phenylene Bis-oxamidate Complexes, *Inorg. Chem.*, 2021, **60**, 9442–9455.
27 Q. Bai, X. Yang, S. Zheng, L. Hong, C. Dai, J. Lin, P. Wang and X. Liang, Efficient electrochemical water oxidation mediated by a binuclear copper complex with a helical structure, *Sustainable Energy Fuels*, 2022, **6**, 3643–3648.
28 M. Bera, K. Keshari, A. Bhardwaj, G. Gupta, B. Mondal and S. Paria, Electrocatalytic Water Oxidation Activity of Molecular Copper Complexes: Effect of Redox-Active Ligands, *Inorg. Chem.*, 2022, **61**, 3152–3165.
29 D. den Boer, A. I. Konovalov, M. A. Siegler and D. G. H. Hetterscheid, Unusual Water Oxidation Mechanism via a Redox-Active Copper Polypyridyl Complex, *Inorg. Chem.*, 2023, **62**, 5303–5314.
30 P. Garrido-Barros, D. Moonshiram, M. Gil-Sepulcre, P. Pelosin, C. Gimbert-Suriñach, J. Benet-Buchholz and A. Llobet, Redox Metal–Ligand Cooperativity Enables Robust and Efficient Water Oxidation Catalysis at Neutral pH with Macrocyclic Copper Complexes, *J. Am. Chem. Soc.*, 2020, **142**, 17434–17446.
31 T. Liu, B. Zhang and L. Sun, Iron-Based Molecular Water Oxidation Catalysts: Abundant, Cheap, and Promising, *Chem. – Asian J.*, 2019, **14**, 31–43.
32 R.-Z. Liao, S. Masaoka and P. E. M. Siegbahn, Metal Oxidation States for the O–O Bond Formation in the Water Oxidation Catalyzed by a Pentanuclear Iron Complex, *ACS Catal.*, 2018, **8**, 11671–11678.
33 F. Acuña-Parés, Z. Codolà, M. Costas, J. M. Luis and J. Lloret-Fillol, Unraveling the Mechanism of Water Oxidation Catalyzed by Nonheme Iron Complexes, *Chem. – Eur. J.*, 2014, **20**, 5696–5707.
34 S. Fukuzumi, Y.-M. Lee and W. Nam, Kinetics and mechanisms of catalytic water oxidation, *Dalton Trans.*, 2019, **48**, 779–798.
35 C.-F. Leung, S.-M. Ng, C.-C. Ko, W.-L. Man, J. Wu, L. Chen and T.-C. Lau, A cobalt(II) quaterpyridine complex as a visible light-driven catalyst for both water oxidation and reduction, *Energy Environ. Sci.*, 2012, **5**, 7903.
36 K. M. Kulesa, D. S. Padilha, B. Thapa, S. Mazumder, Y. Losovyj, H. B. Schlegel, M. Scarpellini and C. N. Verani, A bioinspired cobalt catalyst based on a tripodal imidazole/pyridine platform capable of water reduction and oxidation, *J. Inorg. Biochem.*, 2023, **242**, 112162.
37 A. K. Srivastava, A. Mondal, S. Konar and S. Pal, A tetra Co(ii/iii) complex with an open cubane Co_4O_4 core and square-pyramidal Co(ii) and octahedral Co(iii) centres: bifunctional electrocatalytic activity towards water splitting at neutral pH, *Dalton Trans.*, 2022, **51**, 4510–4521.
38 J.-J. Tan, X.-X. Sun, C.-L. Wang and S.-Z. Zhan, Electrochemical-driven water reduction and oxidation catalyzed by an iron(III) complex supported by a N_2O_2 ligand, *J. Electroanal. Chem.*, 2022, **906**, 115895.
39 L. Quan, H. Jiang, G. Mei, Y. Sun and B. You, Bifunctional Electrocatalysts for Overall and Hybrid Water Splitting, *Chem. Rev.*, 2024, **124**, 3694–3812.

40 J. Yu, T. A. Le, N. Q. Tran and H. Lee, Earth-Abundant Transition-Metal-Based Bifunctional Electrocatalysts for Overall Water Splitting in Alkaline Media, *Chem. – Eur. J.*, 2020, **26**, 6423–6436.

41 X. Zhao, P. Wang and M. Long, Electro- and Photocatalytic Hydrogen Production by Molecular Cobalt Complexes with Pentadentate Ligands, *Comments Inorg. Chem.*, 2017, **37**, 238–270.

42 P. Wang, G. Liang, N. Smith, K. Hill, B. Donnadieu, C. E. Webster and X. Zhao, Enhanced Hydrogen Evolution in Neutral Water Catalyzed by a Cobalt Complex with a Softer Polypyridyl Ligand, *Angew. Chem., Int. Ed.*, 2020, **59**, 12694–12697.

43 M. G. Papanikolaou, A. Elliott, J. McAllister, J. K. Gallos, A. D. Keramidas, T. A. Kabanos, S. Sproules and H. N. Miras, Electrocatalytic hydrogen production by dinuclear cobalt(II) compounds containing redox-active diamidate ligands: a combined experimental and theoretical study, *Dalton Trans.*, 2020, **49**, 15718–15730.

44 P. Garrido-Barros, C. Gimbert-Suriñach, R. Matheu, X. Sala and A. Llobet, How to make an efficient and robust molecular catalyst for water oxidation, *Chem. Soc. Rev.*, 2017, **46**, 6088–6098.

45 J.-W. Wang, P. Sahoo and T.-B. Lu, Reinvestigation of Water Oxidation Catalyzed by a Dinuclear Cobalt Polypyridine Complex: Identification of CoOx as a Real Heterogeneous Catalyst, *ACS Catal.*, 2016, **6**, 5062–5068.

46 H.-Y. Wang, E. Mijangos, S. Ott and A. Thapper, Water Oxidation Catalyzed by a Dinuclear Cobalt–Polypyridine Complex, *Angew. Chem., Int. Ed.*, 2014, **53**, 14499–14502.

47 D. Hong, S. Mandal, Y. Yamada, Y.-M. Lee, W. Nam, A. Llobet and S. Fukuzumi, Water Oxidation Catalysis with Nonheme Iron Complexes under Acidic and Basic Conditions: Homogeneous or Heterogeneous?, *Inorg. Chem.*, 2013, **52**, 9522–9531.

48 J. England, G. J. P. Britovsek, N. Rabadia and A. J. P. White, Ligand Topology Variations and the Importance of Ligand Field Strength in Non-Heme Iron Catalyzed Oxidations of Alkanes, *Inorg. Chem.*, 2007, **46**, 3752–3767.

49 T. Okada, Y. Suzuki, T. Hirose, T. Toda and T. Ozawa, Electro-oxidation of methanol on platinum–organic metal complex mixed catalysts in acidic media, *Chem. Commun.*, 2001, 2492–2493.

50 L. Petit, P. Maldivi and C. Adamo, Predictions of Optical Excitations in Transition-Metal Complexes with Time Dependent-Density Functional Theory: Influence of Basis Sets, *J. Chem. Theory Comput.*, 2005, **1**, 953–962.

51 E. Runge and E. K. U. Gross, Density-Functional Theory for Time-Dependent Systems, *Phys. Rev. Lett.*, 1984, **52**, 997–1000.

52 R. E. Stratmann, G. E. Scuseria and M. J. Frisch, An efficient implementation of time-dependent density-functional theory for the calculation of excitation energies of large molecules, *J. Chem. Phys.*, 1998, **109**, 8218–8224.

53 R. L. Martin, Natural transition orbitals, *J. Chem. Phys.*, 2003, **118**, 4775–4777.

54 J. H. Nelson, L. C. Nathan and R. O. Ragsdale, Complexes of aromatic amine oxides. 4-Substituted quinoline 1-oxide complexes of cobalt(II) and nickel(II) perchlorates, *Inorg. Chem.*, 1968, **7**, 1840–1845.

55 A. E. King, Y. Surendranath, N. A. Piro, J. P. Bigi, J. R. Long and C. J. Chang, A mechanistic study of proton reduction catalyzed by a pentapyridine cobalt complex: evidence for involvement of an anation-based pathway, *Chem. Sci.*, 2013, **4**, 1578.

56 Y. Sun, J. P. Bigi, N. A. Piro, M. L. Tang, J. R. Long and C. J. Chang, Molecular Cobalt Pentapyridine Catalysts for Generating Hydrogen from Water, *J. Am. Chem. Soc.*, 2011, **133**, 9212–9215.

57 J. Niklas, L. Kohler, A. M. Potocny, K. L. Mardis, K. L. Mulfort and O. G. Poluektov, Electronic Structure of Molecular Cobalt Catalysts for H_2 Production Revealed by Multifrequency EPR, *J. Phys. Chem. C*, 2022, **126**, 11889–11899.

58 W. M. Singh, T. Baine, S. Kudo, S. Tian, X. A. N. Ma, H. Zhou, N. J. DeYonker, T. C. Pham, J. C. Bollinger, D. L. Baker, B. Yan, C. E. Webster and X. Zhao, Electrocatalytic and Photocatalytic Hydrogen Production in Aqueous Solution by a Molecular Cobalt Complex, *Angew. Chem., Int. Ed.*, 2012, **51**, 5941–5944.

59 M. Vennampalli, G. Liang, L. Katta, C. E. Webster and X. Zhao, Electronic Effects on a Mononuclear Co Complex with a Pentadentate Ligand for Catalytic H_2 Evolution, *Inorg. Chem.*, 2014, **53**, 10094–10100.

60 D. Basu, S. Mazumder, X. Shi, R. J. Staples, H. B. Schlegel and C. N. Verani, Distinct Proton and Water Reduction Behavior with a Cobalt(III) Electrocatalyst Based on Pentadentate Oximes, *Angew. Chem., Int. Ed.*, 2015, **54**, 7139–7143.

61 K. K. Kpogo, S. Mazumder, D. Wang, H. B. Schlegel, A. T. Fiedler and C. N. Verani, Bimetallic Cooperativity in Proton Reduction with an Amido-Bridged Cobalt Catalyst, *Chem. – Eur. J.*, 2017, **23**, 9272–9279.

62 D. Basu, S. Mazumder, J. Niklas, H. Baydoun, D. Wanniarachchi, X. Shi, R. J. Staples, O. Poluektov, H. B. Schlegel and C. N. Verani, Evaluation of the coordination preferences and catalytic pathways of heteroaxial cobalt oximes towards hydrogen generation, *Chem. Sci.*, 2016, **7**, 3264–3278.

63 M. Rakowski DuBois and D. L. DuBois, The roles of the first and second coordination spheres in the design of molecular catalysts for H_2 production and oxidation, *Chem. Soc. Rev.*, 2009, **38**, 62–72.

64 D. M. Ekanayake, K. M. Kulesa, J. Singh, K. K. Kpogo, S. Mazumder, H. B. Schlegel and C. N. Verani, A pentadentate nitrogen-rich copper electrocatalyst for water reduction with pH-dependent molecular mechanisms, *Dalton Trans.*, 2017, **46**, 16812–16820.

65 D. J. Wasylenko, R. D. Palmer, E. Schott and C. P. Berlinguette, Interrogation of electrocatalytic water oxidation mediated by a cobalt complex, *Chem. Commun.*, 2012, **48**, 2107.

66 D. W. Crandell, S. Ghosh, C. P. Berlinguette and M.-H. Baik, How a $[CoIV–O]^{2+}$ Fragment Oxidizes Water: Involvement of a Biradicaloid $[CoII–(^{\bullet}O^{\bullet})]^{2+}$ Species in Forming the O–O Bond, *ChemSusChem*, 2015, **8**, 844–852.
67 B. Das, A. Orthaber, S. Ott and A. Thapper, Water oxidation catalysed by a mononuclear CoII polypyridine complex; possible reaction intermediates and the role of the chloride ligand, *Chem. Commun.*, 2015, **51**, 13074–13077.
68 D. K. Dogutan, R. McGuire and D. G. Nocera, Electocatalytic Water Oxidation by Cobalt(III) Hangman β-Octafluoro Corroles, *J. Am. Chem. Soc.*, 2011, **133**, 9178–9180.

